JACS Au
AN OPEN ACCESS JOURNAL OF THE AMERICAN CHEMICAL SOCIETY

pubs.acs.org/jacsau

Article

Modulating Uranium Extraction Performance of Multivariate Covalent Organic Frameworks through Donor–Acceptor Linkers and Amidoxime Nanotraps

Mengjie Hao, Yinghui Xie, Xiaolu Liu, Zhongshan Chen, Hui Yang,* Geoffrey I. N. Waterhouse, Shengqian Ma,* and Xiangke Wang*

Cite This: *JACS Au* 2023, 3, 239–251

Read Online

ACCESS | Metrics & More | Article Recommendations | Supporting Information

ABSTRACT: Covalent organic frameworks (COFs) can be designed to allow uranium extraction from seawater by incorporating photocatalytic linkers. However, often sacrificial reagents are required for separating photogenerated charges which limits their practical applications. Herein, we present a COF-based adsorption-photocatalysis strategy for selective removal of uranyl from seawater in the absence of sacrificial reagents. A series of ternary and quaternary COFs were synthesized containing the electron-rich linker 2,4,6-triformylphloroglucinol as the electron donor, the electron-deficient linker 4,4′-(thiazolo[5,4-*d*]thiazole-2,5-diyl)dibenzaldehyde as the acceptor, and amidoxime nanotraps for selective uranyl capture (with the quaternary COFs incorporating [2,2′-bipyridine-5,5′-diamine-Ru(Bp)$_2$]Cl$_2$ as a secondary photosensitizer). The ordered porous structure of the quaternary COFs ensured efficient mass transfer during the adsorption-photocatalysis capture of uranium from seawater samples, with photocatalytically generated electrons resulting in the reduction of adsorbed U(VI) to U(IV) in the form of UO_2. A quaternary COF, denoted as COF 2-Ru-AO, possessed a high uranium uptake capacity of 2.45 mg/g/day in natural seawater and good anti-biofouling abilities, surpassing most adsorbents thus far. This work shows that multivariate COF adsorption-photocatalysts can be rationally engineered to work efficiently and stably without sacrificial electron donors, thus opening the pathway for the economic and efficient extraction of uranium from the earth's oceans.

KEYWORDS: *multivariate covalent organic frameworks, chelating affinity, adsorption-photocatalysis, donor–acceptor, uranium extraction*

INTRODUCTION

Uranium (^{235}U) is the main fuel used in nuclear fission reactors.[1,2] Currently, it is produced by enrichment of uranium extracted from terrestrial uranium-rich ores (99.3% ^{238}U, 0.7% ^{235}U). However, uranium ore reserves on land are limited, representing a major bottleneck in the future proliferation of nuclear power. Accordingly, research interest is now being directed toward recovering uranium from seawater to satisfy expected future demand.[3] The earth's oceans contain approximately 3.3 micrograms per liter of uranium, representing a total uranium amount more than 1000 times that on land. However, selective uranium extraction from seawater is challenging owing to the presence of a large number of co-dissolved metal ions and microorganisms.[4,5]

With a view toward harvesting marine uranium resources, it is essential to develop materials that can resist biofouling and selectively capture uranium under high ionic strength conditions. Adsorbent materials such as porous carbon-based adsorbents,[6−12] layered organic–inorganic materials,[13] organic polymers,[14−25] biomaterials,[26−28] and metal–organic frameworks (MOFs)[29−34] have all been investigated for uranium extraction from seawater. However, these adsorbents possess drawbacks, including one or more of the following: slow adsorption kinetics, low adsorption capacities, poor stability, inferior recyclability, or rapid marine biological passivation. Accordingly, they are not suitable for long-term uranium capture.

Covalent organic frameworks (COFs), as an emerging type of crystalline porous material, are garnering increasing interest as adsorbents due to their low cost and unique structural characteristics including tunable porosity, large surface area, relatively low density, and tunable functionality.[35−41] By judicious choice of linker components, COFs with specific properties can be synthesized for target applications. As an example, amidoxime-functionalized COFs have been shown to offer a high affinity toward uranium in seawater, proving one of the best uranyl adsorbents reported to date.[42−44] However,

Received: November 10, 2022
Revised: December 23, 2022
Accepted: December 23, 2022
Published: January 4, 2023

https://doi.org/10.1021/jacsau.2c00614
JACS Au 2023, 3, 239–251

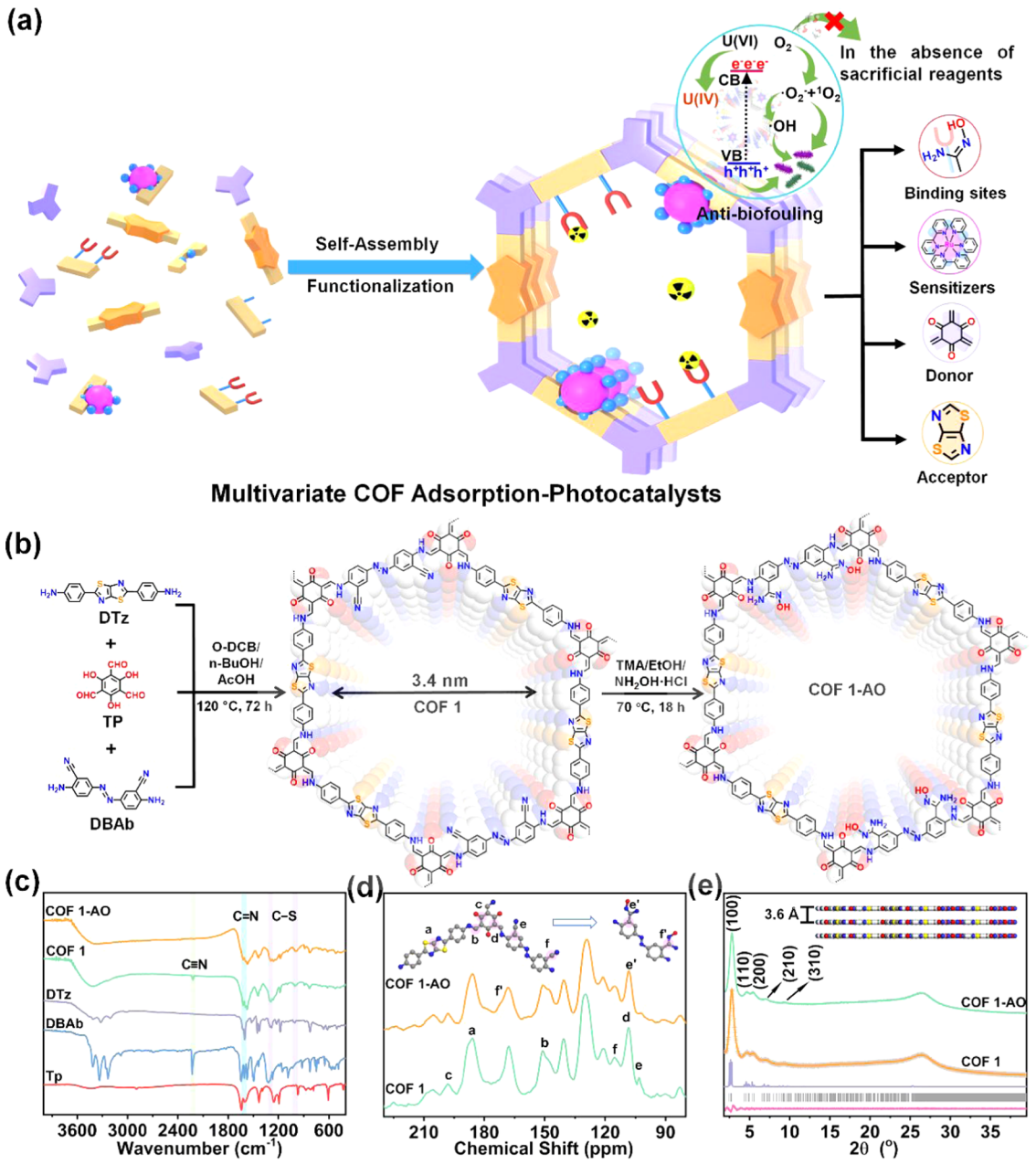

Figure 1. Schematic, preparation, and characterization of multivariate COFs. (a) Schematic of a multivariate COF equipped with amidoxime nanotraps, photocatalytic donor−acceptor sites, and anti-biofouling properties as an adsorption-photocatalyst for uranium extraction from seawater (without the need for sacrificial reagents). (b) Synthetic scheme for COF 1, and its corresponding postsynthetic modification to chemically transform cyano groups to amidoxime groups, yielding COF 1-AO. (c) FTIR spectra of COF 1, COF 1-AO, and linkers. (d) Solid-state ^{13}C CP/MAS NMR spectra of COF 1 and COF 1-AO. (e) Experimental and simulated PXRD profiles (inset: graphical view of the eclipsed AA stacking structure of COF 1-AO). C, N, O, and S atoms are represented by gray, blue, red, and yellow, respectively. The H atoms are omitted for clarity.

when used simply as a uranyl adsorbent, simple amidoxime-functionalized COFs have the drawback that elution of adsorbed uranyl generally requires harsh conditions, which can damage the amidoxime binding sites and the porous structure of the COF, thus limiting practical implementation. In recent contributions, incorporating photoactive components into the linkers in COFs has been shown to improve uranium extraction from seawater and other applications.[43,45−55] However, in these studies, large amounts of sacrificial electron donors were needed as sacrificial hole scavengers (reducing viability as a practical uranium capture technology). COFs need to be discovered that are capable of efficiently capturing uranium from seawater and photocatalytically reducing U(VI) to solid products such as UO_2 for collection without the need for sacrificial reagents.

Multivariate COFs are composed of three or more sets of linkers, and often exhibit properties that do not exist in their single- or two-component counterparts.[56−58] In particular, tuning the spatial environment and functional linkers of multivariate COFs allows properties be optimized for target applications. Inspired by this attractive attribute, we herein used reticular chemistry to synthesize COFs with adsorption-photocatalytic properties for efficient uranium extraction from seawater under visible light irradiation without the need for

https://doi.org/10.1021/jacsau.2c00614
JACS Au 2023, 3, 239−251

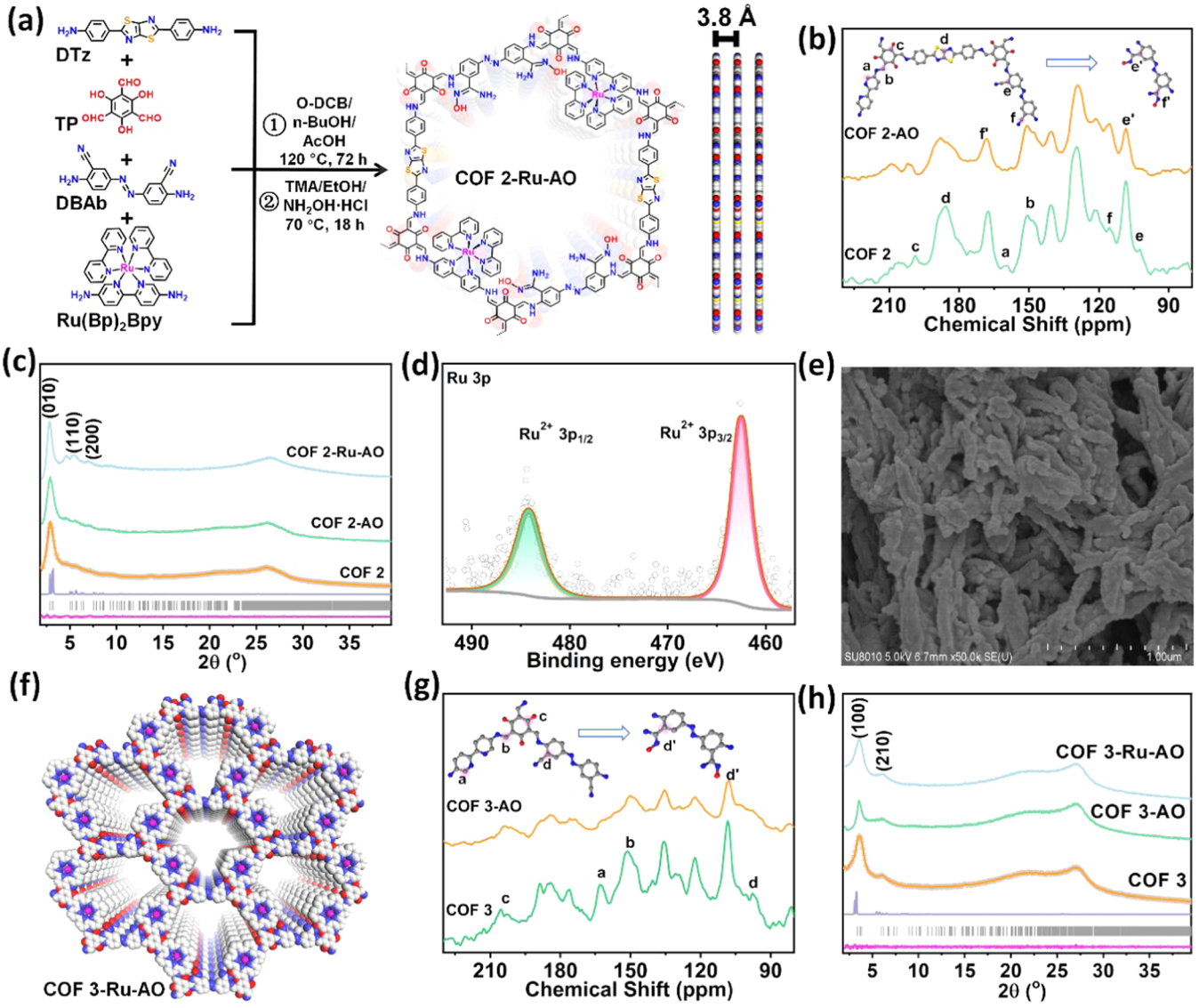

Figure 2. Preparation and characterization of COF 2, COF 2-AO, COF 2-Ru-AO, COF 3, COF 3-AO, and COF 3-Ru-AO. (a) Synthetic scheme for COF 2-Ru-AO. (b) Solid-state ^{13}C CP/MAS NMR spectra of COF 2 and COF 2-AO. (c) Experimental and simulated PXRD profiles of COF 2, COF 2-AO, and COF 2-Ru-AO. (d) Ru 3p XPS spectrum for COF 2-Ru-AO. (e) SEM image of COF 2-Ru-AO. (f) Graphic view of the eclipsed AA stacking structure of COF 3-Ru-AO. (g) Solid-state ^{13}C CP/MAS NMR spectra of COF 3 and COF 3-AO. (h) Experimental and simulated PXRD profiles of COF 3, COF 3-AO, and COF 3-Ru-AO. C, N, O, S, and Ru atoms are represented by gray, blue, red, yellow, and magenta spheres, respectively. H atoms are omitted for clarity.

any sacrificial reagents. Our strategy involved the creation of multivariate COFs with donor−acceptor sites and amidoxime nanotraps (Figure 1a). The high crystallinity, large porosity, good chemical stability, excellent light-harvesting ability, efficient electron−hole separation ability, and good anti-biofouling properties of one of our quaternary COFs (denoted herein as COF 2-Ru-AO) enabled selective capture of uranium with a record-high uranium extraction efficiency ~2.45 mg/g per day among all COF adsorbents and photocatalysts from natural seawater in the absence of any sacrificial reagents. The findings and mechanistic insights presented inform the rational design and synthesis of multivariate COFs with outstanding performance for uranium extraction.

RESULTS AND DISCUSSION

COFs Synthesis and Structural Characterization

The geometric and chemical characteristics of the pores in COFs determine their functional properties. On the basis that thiazole-based ligands show excellent abilities for charge-transport in photocatalytic applications,[45,54] and amidoxime functional groups exhibit affinity for uranyl,[23,43,44] our initial step was to build amidoxime and thiazole-containing moieties into a three component COF (Figure 1b). Considering that amidoxime groups could be derived from cyano groups through the hydrolysis reaction with hydroxylamine, a nitrile-functionalized COF (COF 1) was first synthesized via the solvothermal reaction of 2,4,6-triformylphloroglucinol (TP), 4,4′-(thiazolo[5,4-*d*]thiazole-2,5-diyl)dianiline (DTz), and 5,5′-(diazene-1,2-diyl)bis(2-aminobenzonitrile) (DBAb) in an acetic acid (AcOH)/1,2-dichlorobenzene (O-DCB)/1-butanol

https://doi.org/10.1021/jacsau.2c00614
JACS Au 2023, 3, 239−251

(n-BuOH) mixed solvent at 120 °C. The structure of COF 1 was determined by Fourier transform infrared spectroscopy (FTIR), solid-state ^{13}C NMR spectroscopy, powder X-ray diffraction (PXRD), and Material Studio theoretical simulations. The disappearance of −CHO peak at 1640 cm^{-1} and $-NH_2$ stretches at 3600−3050 cm^{-1} in the FTIR spectra indicated the complete reaction of the ligands (Figure 1c). Furthermore, the peak at 2224 cm^{-1} confirmed the retention of the cyano group on the DBAb linker. The solid-state ^{13}C NMR spectrum revealed a new C═O peak at 198 ppm verifying the formation of β-ketoenamine moieties (Figure 1d).[59,60] Moreover, the observed characteristic peak at ∼185 ppm in the solid-state ^{13}C NMR spectrum confirmed the presence of the DTz linker in the COF 1 structure (Figure 1d). Further, the presence of C−S stretching bands at ∼1001 and 1295 cm^{-1} in the FTIR spectrum of COF 1 also confirmed the presence of the DTz linker (Figure 1c). The experimental PXRD pattern showed the peaks at 2θ angles of 2.73, 4.63, 5.41, 6.97, and 9.33°, corresponding to (100), (110), (200), (210), and (310) reflections, respectively (Figure 1e). A plausible theoretical crystalline structure was built through the simulation of the experimental PXRD pattern by Materials Studio software.[61] The refined unit cell parameters for COF 1 were determined as a = 36.46 Å, b = 38.87 Å, c = 3.52 Å, $\alpha = \beta$ = 90°, and γ = 114.75°, with agreement factors of R_p = 1.25% and R_{wp} = 1.60% (Tables S1 and S2). Taking these results into account, an eclipsed AA stacking two-dimensional (2D) structure with 3.4 nm hexagonal 1D open channels was obtained (Figures 1b and S1a). The side view showed the $\pi-\pi$ stacking distance between individual layers to be ∼3.6 Å (Figure 1e). Thermogravimetric analysis (TGA) demonstrated that the framework is stable up to ∼300 °C (Figure S6). Next, COF 1 underwent an amidoximation process, yielding our target product COF 1-AO, with the ligand functional amidoxime groups located in large pores (Figures 1b and S1b). PXRD showed that the crystallinity of COF 1 was retained after amidoxime functionalization (Figure 1e). The disappearance of the nitrile stretching band at 2224 cm^{-1} in the FTIR spectrum revealed the successful transformation of the −CN group in COF 1 to the amidoxime group in COF 1-AO (Figure 1c). Solid-state ^{13}C NMR analysis further confirmed this derivatization by the disappearance of −CN signals at ∼103 ppm (Figure 1d). Scanning electron microscopy (SEM) imaging of COF 1 and COF 1-AO revealed nanofiber morphologies (Figures S9 and S10). On the basis of data collected using complementary characterization techniques and theoretical simulations, we established that COF 1-AO is composed of three components, including amidoxime uranium nanotraps, DTz electron acceptors together with β-ketoenamine (derived from TP linker) electron donors. The structural features were expected to create an efficient adsorption-photocatalyst for uranium extraction from seawater.

$[Ru(Bp)_3]^{2+}$ (Bp = 2,2′-bipyridine) is widely used as a photosensitizer to introduce photocatalytic function in COFs and other coordination polymers.[62,63] Inspired by our success synthesizing COF 1-AO, we aimed to optimize the multi-electron transfer efficiency of our multivariate COFs by introducing $[Ru(Bp)_x]^{2+}$, thus creating a highly efficient adsorption-photocatalyst system for uranium extraction studies. Accordingly, a quaternary component COF was solvothermally synthesized via an imine condensation of TP, [2,2′-bipyridine-5,5′-diamine-$Ru(Bp)_2$]Cl_2 (a Ru-functionalized ligand, $[Ru(Bp)_2Bpy]Cl_2$), DBAb, and DTz in an n-BuOH/O-DCB/AcOH solvent mixture at 120 °C for 72 h (Figure 2a). This produced COF 2-Ru. Owing to the low symmetry and complexity of the $[Ru(Bp)_2Bpy]Cl_2$ ligand in COF 2-Ru, a simpler isostructural analogue COF 2 was synthesized to determine and investigate the structure of COF 2-Ru and its amidoxime derivative COF 2-Ru-AO. COF 2 was prepared using the same protocol, except that $[Ru(Bp)_2Bpy]Cl_2$ was replaced with the 2,2′-bipyridine-5,5′-diamine (Bpy) ligand. FTIR spectroscopy showed a similar peak at ∼1286 cm^{-1} in both COFs, confirming the successful formation of C−N bonds in the structures (Figure S16). The peak ∼2224 cm^{-1} is ascribed to a −CN stretching band from the DBAb linker. Analysis of the solid-state ^{13}C NMR spectrum gave evidence of pyridine and thiazole ring signals at ∼160 and ∼185 ppm, respectively, indicating the successful incorporation of the two ligands (Figure 2b). In addition, the presence of peaks at 103 and 198 ppm confirmed −CN and keto (C═O) groups, respectively. PXRD verified the formation of a periodic crystalline structure. The experimental PXRD pattern of COF 2 matched well with the theoretical simulation for an eclipsed AA stacking structure (Figure 2c), indicating the phase purity of COF 2. COF 2 crystallizes in a monoclinic P1 space group with unit cell parameters of a = 34.26 Å, b = 37.35 Å, and c = 3.74 Å, α = 108.89°, β = 83.47°, and γ = 126.28° (Tables S1 and S3). Comparison of PXRD patterns showed COF 2-Ru to possess a similar space group, crystallinity and purity as COF 2 (Figures 2c and S18), evidence that both COFs were isostructural. The functional Ru-bipyridine units are located in the large pores of the COF 2-Ru framework (Figure S3). The obtained COF 2 and COF 2-Ru then underwent postsynthetic modification to transform the cyano groups into amidoxime groups, yielding COF 2-AO and COF 2-Ru-AO, respectively. PXRD patterns determined that the crystallinity and structure of the frameworks were retained after the amidoxime functionalization step (Figure 2c). Solid-state ^{13}C NMR showed that the −CN groups in the parent COF were completely transformed into amidoxime groups (Figure 2b). COF 2-Ru-AO showed a similar structure to COF 2-AO (Figure S3). SEM images of COF 2-Ru-AO, COF 2, and COF 2-AO powder samples showed similar nanoscale morphologies (Figures 2e, S11, and S12). High-angle annular dark-field scanning transmission electron microscopy (HAADF-STEM) and corresponding elemental mapping images showed a uniform distribution of the C, N, S, O, Ru, and Cl in COF 2-Ru-AO, indicating that the Ru component was successfully incorporated onto the COF (Figure S13). X-ray photoelectron spectroscopy (XPS) further confirmed the existence of Ru and Cl elements (Figure S22). The binding energy of the Ru $3d_{5/2}$ XPS signal at 280.8 eV suggested a Ru^{2+} species (Figure S23).[62] The Ru $3p_{3/2}$ and Ru $3p_{1/2}$ signals at 462.5 and 484.3 eV provided further strong evidence for the presence of Ru(II) in the functionalized framework (Figure 2d).

In the studies below, COF 1-AO, COF 2-AO, and COF 2-Ru-AO were evaluated as adsorbents and adsorption-photocatalysts for uranium extraction from seawater solutions in the absence of sacrificial reagents. For context, a further reference framework COF 3-Ru-AO was synthesized by combining TP, DBAb, and $[Ru(Bp)_2Bpy]Cl_2$ linkers under similar synthesis and amidoxime functionalization conditions as used to prepare the other COFs. The detailed synthetic procedure and characterizations are provided in the Figure 2f−h and

https://doi.org/10.1021/jacsau.2c00614
JACS Au 2023, 3, 239−251

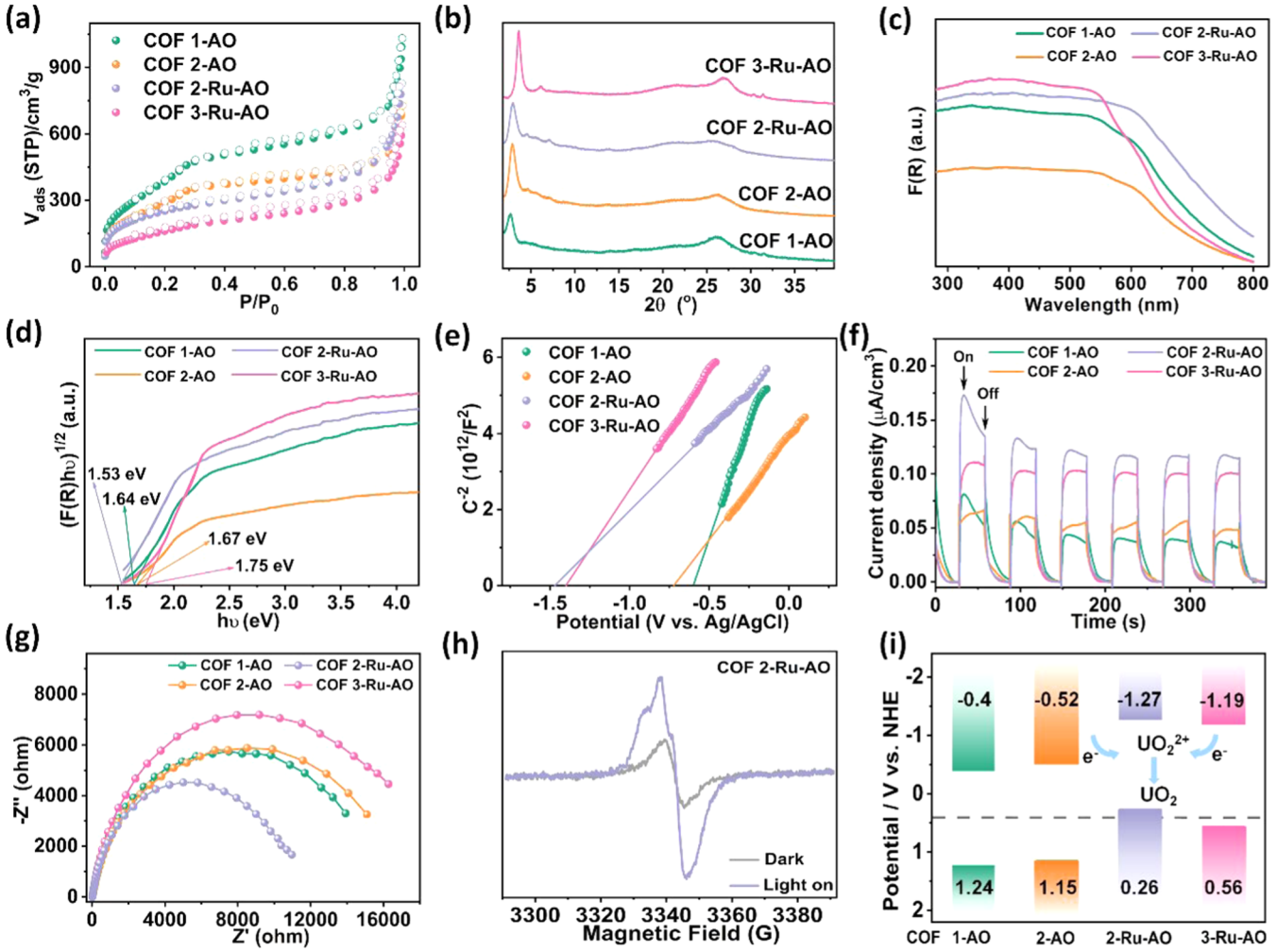

Figure 3. Characterization of synthesized COFs. (a) N_2 sorption isotherms measured at 77 K for different COFs. (b) PXRD patterns for COFs after treatment in seawater for 24 h. (c, d) UV−visible diffuse reflectance spectra and corresponding band gap estimation for different COFs. (e) Mott−Schottky plots for different COFs. (f) Photocurrent responses of different COFs under visible light irradiation. (g) Electrochemical impedance spectra (EIS) of different COFs. (h) EPR spectra for COF 2-Ru-AO under dark and light conditions. (i) Band edge positions for different COFs vs the normal hydrogen electrode (NHE). Potential for UO_2^{2+}/UO_2 reduction couples is indicated.

Supporting Information (Figures S4, S5, S8, S14, S15, S17, and S24−S26). Characterization studies using FTIR, solid-state ^{13}C NMR, PXRD, SEM, XPS, and theoretical structure simulations confirmed the successful incorporation of the three components in COF 3-Ru. Furthermore, the PXRD patterns of COF 3-Ru and COF 3-Ru-AO closely matched that of the parent COF 3 framework, confirming that all three COFs were isostructural and phase pure.

Porosity, Chemical Stability, and Electrochemical and Photoelectrochemical Properties

The porosities of the multivariate COFs were probed by nitrogen adsorption−desorption studies at 77 K. The N_2 uptake capacities, pore volume, BET surfaces, and corresponding pore size distributions are summarized in Table S5, Figures 3a and S27−S32. The adsorption−desorption curves showed characteristic type II isotherms, indicating that both micropores and small mesopores were present in the COFs, consistent with their crystal structures (Figure 3a). Among these materials, COF 2-Ru-AO offered a maximum N_2 uptake capacity of 828 cm^3/g and a BET surface area of 896.8 m^2/g, indicating the retention of significant porosity after Ru-bipyridine functionalization. The chemical stabilities of the COFs were next evaluated by soaking the samples in HCl (pH 1), NaOH (pH 12), and natural seawater over 24 h. PXRD patterns revealed no framework collapse or undesirable phase transitions occurred under any of these conditions (Figures 3b and S19−S21).

The optical, electrochemical, and photoelectrochemical properties of the developed multivariate COFs were studied by ultraviolet/visible diffuse reflectance spectroscopy (UV/vis DRS), Mott−Schottky plots, photocurrent measurements, electrochemical impedance spectroscopy (EIS), and electron paramagnetic resonance (EPR) spectroscopy. UV/vis DRS spectra showed all COFs to have band gaps in the visible range (Figure 3c,d), with calculated band gap energies of 1.64, 1.67, 1.53, and 1.75 eV for COF 1-AO, COF 2-AO, COF 2-Ru-AO, and COF 3-Ru-AO, respectively. COF 2-Ru-AO had the narrowest band gap, thus requiring the least energy to create charge carriers. Conduction band positions determined by measuring the flat band potential (E_{fb}) from Mott−Schottky plots (Figure 3e,i) were −0.6, −0.72, −1.47, and −1.39 V (vs Ag/AgCl) for COFs 1-AO, 2-AO, 2-Ru-AO, and 3-Ru-AO, respectively. COF 2-Ru-AO exhibited the strongest photocurrent response (Figure 3f) and the smallest semicircle

https://doi.org/10.1021/jacsau.2c00614
JACS Au 2023, 3, 239−251

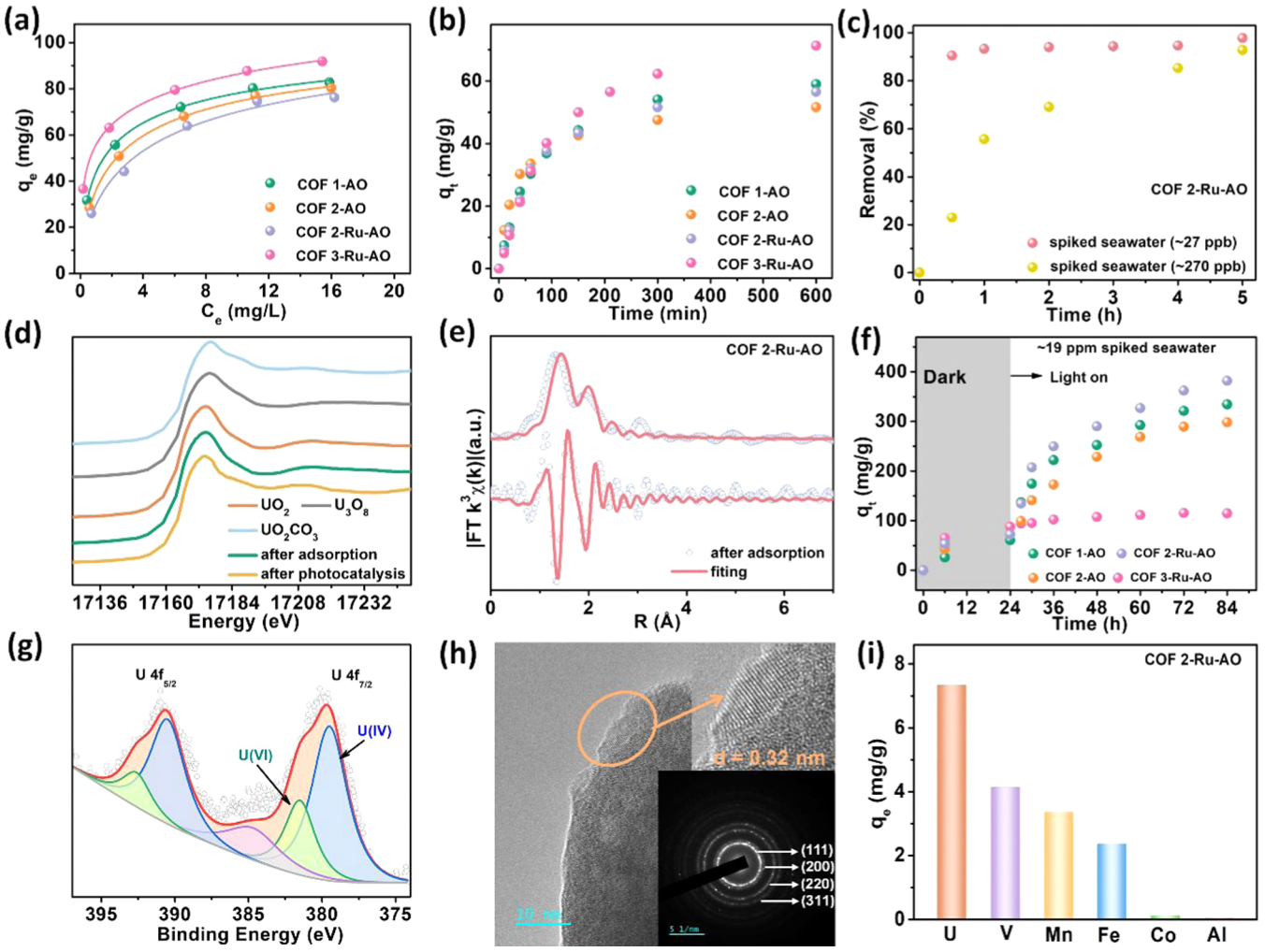

Figure 4. Uranium extraction isotherms, kinetics, EXAFS, XANES, XPS, and TEM results. (a) Equilibrium adsorption isotherms for uranium adsorption on different COF materials in uranyl-spiked seawater (uranium concentrations ranging from ~2 to ~20 ppm; fit lines for the Langmuir model are shown). (b) Uranyl adsorption kinetics on different COF materials at an initial uranium concentration of ~9 ppm in uranyl-spiked seawater. (c) Uranyl adsorption kinetics on COF 2-Ru-AO at an initial uranium concentration of ~27 and 270 ppb in uranyl-spiked seawater, respectively. (d) U L_{III}-edge XANES spectra for COF 2-Ru-AO after uranium adsorption and photocatalysis studies. UO_2, U_3O_8, and UO_2CO_3 are employed for comparison (the data for UO_2, U_3O_8, and UO_2CO_3 in (d) were reported in our previous work[9,53]). (e) U L_{III}-edge EXAFS plots and corresponding fitting curves for COF 2-Ru-AO after adsorption of uranium. (f) Uranium extraction from spiked seawater with initial uranium concentrations of ~19 ppm, using COFs 1-AO, 2-AO, 2-Ru-AO, and 3-Ru-AO as adsorbent-photocatalysts. (g) U 4f XPS spectrum of COF 2-Ru-AO after photocatalysis. (h) HRTEM image and SAED pattern of a solid UO_2 nanoparticle on COF 2-Ru-AO after the adsorption-photocatalysis study. (i) Selectivity of COF 2-Ru-AO for metals in natural seawater (72 h).

diameter in the EIS Nyquist plots among the COFs synthesized in this work (Figure 3g), indicating that COF 2-Ru-AO possessed superior charge separation properties. Accordingly, light-induced charge carrier generation was further investigated using electron paramagnetic resonance (EPR) spectroscopy. A signal was observed at $g = 2.004$ due to unpaired electrons in the conduction band (Figure 3h). The signal intensified greatly upon visible light irradiation of COF 2-Ru-AO, indicating that electrons jumped from the valence band to the conduction band (i.e., charge carrier generation). Intuitively, this suggested that COF 2-Ru-AO should deliver superior photocatalytic performance relative to the other COFs, which was validated by experiment below. Importantly, the conduction band positions of all of the COFs were greater than the potential of U(VI)/U(IV) redox couple (0.411 V vs NHE), suggesting that COFs would be capable of reducing adsorbed U(VI) to U(IV) products such as UO_2 under visible light irradiation. This suggested suitability for the adsorption-photocatalytic extraction of uranium from seawater.[64]

Uranium Adsorption Studies

Encouraged by the aforementioned results, we anticipated that our adsorption-photocatalyst COF design strategy would confer significant benefits in extracting uranium from seawater due to (i) large porosity and excellent chemical stabilities under acid, basic, and high ionic strength conditions; (ii) amidoxime nanotraps with strong uranyl binding affinity; (iii) the framework donor (TP and bipyridine-Ru(II))-acceptor (DTz linker) system that would allow efficiently separation of photogenerated electrons and holes, thus allowing photocatalytic reduction of adsorbed U(VI) to lower valance products such as solid U(IV)O_2; and (iv) bipyridine-Ru(II) sites served as secondary photosensitizer for enhanced photocatalytic performance. Therefore, we conducted a series of experiments to assess the uranium extraction performance

https://doi.org/10.1021/jacsau.2c00614
JACS Au 2023, 3, 239−251

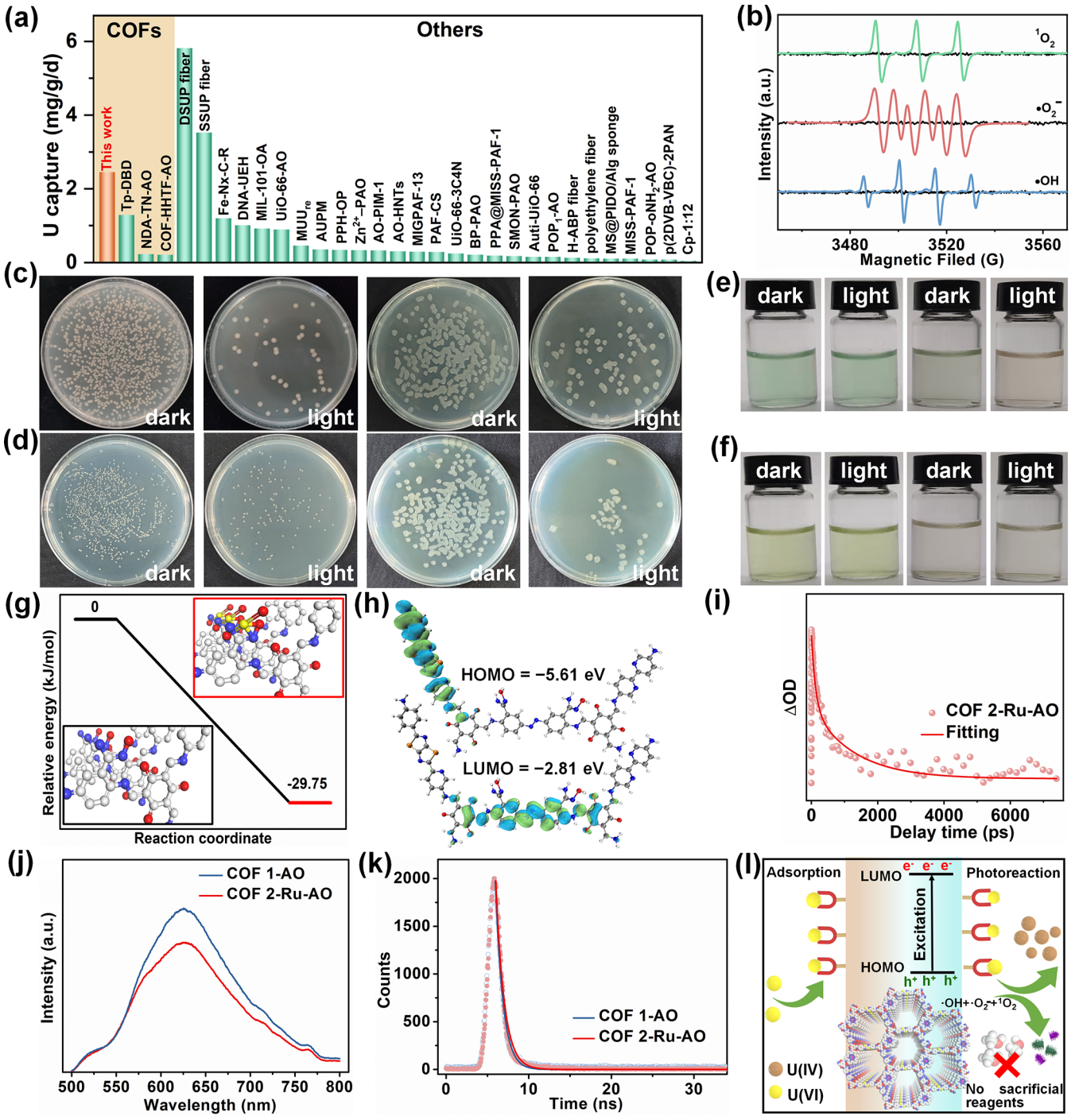

Figure 5. Uranium extraction performance comparison, EPR analysis, anti-biofouling activity, TAS, PL, time-resolved PL spectra, and computational studies of COF 2-Ru-AO. (a) Comparison of uranium extraction uptake performance of COF 2-Ru-AO and other reported materials in natural seawater. (b) EPR spectra for •O$_2^-$-DMPO, •OH-DMPO, and ^{1}O$_2$-TEMP complexes formed under visible light irradiation of COF 2-Ru-AO. Black lines show corresponding data obtained under dark conditions. The •OH radicals were likely generated from •O$_2^-$ via the •O$_2^-$ → H$_2$O$_2$ → •OH + OH$^-$ pathway since the valence band holes generated in COF 2-Ru-AO are not able to directly oxidize water to •OH.[69,70] (c) Photographs of marine bacteria (left two) and *Bacillus indicus* (right two) after treatment with COF 2-Ru-AO in the dark and under visible light conditions. (d) Photographs of *Vibrio vulnificus* (left two) and *Pseudomonas stutzeri* (right two) colonies after treatment with COF 2-Ru-AO in the dark and under visible light conditions. (e) Photographs of *Synechococcus elongatus* without catalyst (top left two) and treated with COF 2-Ru-AO (right two) under dark and visible light conditions. (f) Photographs of *Chlorella sorokiniana* without catalyst (left two) and treated with COF 2-Ru-AO (right two) under dark and visible light conditions, respectively. (g) DFT-optimized structure of UO_2^{2+}/COF 2-Ru-AO and the corresponding binding free energy. (h) Computational studies of molecular orbital adiabatic potentials for COF 2-Ru-AO. (i) Transient absorption spectrum of COF 2-Ru-AO (at λ_{ex} = 490 nm). (j) Photoluminescence spectra of COF 2-Ru-AO and COF 1-AO (excitation at 340 nm). (k) Time-resolved photoluminescence spectra of COF 2-Ru-AO and COF 1-AO (excitation at 320 nm). (l) Proposed mechanism of COF 2-Ru-AO for photocatalysis. C, N, O, S, U, and H atoms are represented by gray, blue, red, orange, yellow, and white spheres, respectively, in (g), (h), and (l). The [Ru(Bp)$_2$]Cl$_2$ component has been omitted for clarity in (g) and (h).

https://doi.org/10.1021/jacsau.2c00614
JACS Au 2023, 3, 239−251

and durability of the various multivariate COFs described above.

We first evaluated the uranium adsorption ability of the various multivariate COFs in spiked seawater solutions at pH 8.1. Using initial uranium concentrations ranging from ∼2 to ∼20 ppm at 298 K, the calculated maximum adsorption capacities of COF 1-AO, COF 2-AO, COF 2-Ru-AO, and COF 3-Ru-AO were determined to be 82.8, 80.4, 76.2, and 91.8 mg/g, respectively (Figure 4a). These values were comparable to other high-performance adsorbents under similar conditions. Moreover, the adsorption isotherms were fitted well by the Langmuir model indicating that the introduced amidoxime functional groups offered excellent affinities toward uranyl (Table S6). The adsorption kinetics were studied in ∼9 ppm spiked seawater solutions over periods ranging from 0 to 10 h. All COFs showed fast initial adsorption kinetics with adsorption equilibrium reached in ∼300 min (Figure 4b). The adsorption kinetics are well described by the pseudo-second-order model, with high R^2 values obtained (Table S7, Figures S33−S36). The results are explained by uranyl adsorption at amidoxime nanotraps, resulting in highly selective adsorption. We carried out further adsorption experiments in ∼27 and ∼270 ppb uranyl-spiked seawater solutions using COF 2-Ru-AO. The experiments revealed a super-fast uranium uptake at low concentrations, reaching over 95 and 92%, respectively, of their equilibrium adsorption capacity within 5 h (Figure 4c). The results highlight the outstanding properties of COF 2-Ru-AO for the selective adsorption of uranium at low concentrations in seawater.

U L_{III}-edge X-ray absorption near edge structure (XANES) and extended X-ray absorption fine structure (EXAFS) studies were performed to probe the uranyl coordination environment in COF 2-Ru-AO after uranium adsorption (the data can be considered representative for all of the other COFs studied in this work). U L_{III}-edge XANES showed COF 2-Ru-AO to bind uranyl in the form of U(VI), with the data collected being very similar to that of the $U(VI)O_2CO_3$ reference (Figure 4d). The Fourier transformed U L_{III}-edge EXAFS (Figure 4e) showed peaks at 1.45 and 1.91 Å in R-space, corresponding to $U-O_{ax}$ and a mixture of $U-O_{eq.1}$ + $U-O_{eq.2}(N)$ scattering paths, respectively. Fitting the spectrum confirmed that COF 2-Ru-AO binds U(VI) in an uranyl-amidoxime η^2-binding mode (Figure S41 and Table S8).[44,65]

Photocatalytic Uranium Extraction Studies

Encouraged by the excellent uranium adsorption performance and unique structural features of the COFs, we next evaluated the photocatalytic uranium extraction properties of the COFs in spiked seawater. Before testing, the COFs were immersed in ∼19 ppm uranyl-spiked seawater at 25 °C for 24 h to allow uranium adsorption equilibrium to be established. The adsorption-photocatalysis data obtained is summarized in Figure 4f. COF 1-AO, COF 2-AO, and COF 2-Ru-AO achieved uranium extraction capacities of 334.4, 298.4, and 382.0 mg/g, respectively, in the absence of any sacrificial reagent in 84 h. The removal efficiency of COF 2-Ru-AO was therefore 7.0 and 13.6% higher than that of COF 1-AO and COF 2-AO, respectively, confirming the superior adsorption-photocatalysis performance of COF 2-Ru-AO (suggesting that the introduction of bipyridine-Ru(II) groups in the COF structure boosted the photocatalytic activity). In comparison, COF 3-Ru-AO showed no photocatalytic activity under similar conditions, highlighting the importance of donor−acceptor pairs in COFs 1-AO, 2-AO, and 2-Ru-AO, which allowed efficient separation of electrons and holes without any need for sacrificial reagents during photocatalysis. We subsequently performed XPS, U L_{III}-edge XANES, and TEM analyses to characterize the products generated in the adsorption-photocatalytic process. Analysis of the U L_{III}-edge XANES spectrum showed a pre-edge similar to that of UO_2, indicating that U(IV) was present after photocatalysis (Figure 4d). The U 4f XPS spectrum further confirmed these results (Figure 4g).[43,66] HAADF-STEM and elemental mapping images showed a uniform distribution of uranium and oxygen on the surface of COF support after photocatalysis (Figure S37). The HRTEM image of an individual nanoparticle on the surface of COF 2-Ru-AO after photocatalysis showed lattice fringes with an interplanar spacing of 0.32 nm, corresponding to the (111) planes of cubic UO_2 (Figure 4h). The corresponding selected area electron diffraction (SAED) pattern showed rings that could be indexed to the (111), (200), (220), and (311) planes of solid UO_2. COF 2-Ru-AO maintained a uranium removal efficiency as high as 88.3% after five recycle runs, indicating excellent durability and reusability (Figure S38). PXRD confirmed the structure of COF 2-Ru-AO was retained after the recycling tests (Figure S39). To our knowledge, this is the first time a multivariate COF adsorption-photocatalyst has been used to capture U(VI) from seawater and yield a U(IV) solid product under visible light irradiation in the absence of sacrificial reagents.

Adsorption-Photocatalytic Extraction of Uranium from Natural Seawater

Inspired by the findings above, we next conducted uranium extraction studies on COF 2-Ru-AO in natural seawater (Figure S40). A uranium extraction capacity of 7.36 mg/g over 72 h (an average of 2.45 mg/g per day) was achieved under visible light irradiation (Figure 4i). The extraction performance of COF 2-Ru-AO compared very favorably with other high-performing adsorbents or technologies reported in the literature, demonstrating the great promise for practical applications (Figure 5a and Table S9). Furthermore, ICP-MS analysis showed that the vanadium uptake capacity was only 4.14 mg/g after 72 h (an average of 1.38 mg/g per day), with the calculated uranium/vanadium removal selectivity reaching 2.9 (Figure 4i and Table S10), indicating an excellent extraction selectivity for uranium relative to vanadium. Minimizing competitive vanadyl adsorption is a key factor in designing adsorbents for uranium extraction from seawater. Most amidoxime-based adsorbents reported to date showed poor uranium/vanadium selectivities,[22,43,67,68] thus the adsorption-photocatalyst COF 2-Ru-AO is among the best materials yet developed for seawater uranium sequestration. COF 2-Ru-AO also showed excellent selectivity for uranium against other metal ions (including Fe^{3+}, Co^{2+}, Al^{3+}, Ni^{2+}, Ca^{2+}, Mg^{2+}, Mn^{2+}, K^+, and Na^+) under high ionic strength conditions (Table S10).

Anti-Biofouling Activity of COF 2-Ru-AO

Biofouling can degrade the uranium extraction efficiency of adsorbents by passivating adsorption sites, thus reducing its usefulness for practical applications. Accordingly, we further studied the anti-biofouling properties of COF 2-Ru-AO by measuring its ability to inhibit marine bacteria, *B. indicus*, *V. vulnificus*, *P. stutzeri*, and algae (*S. elongates* and *C. sorokiniana*) before and under visible light irradiation in natural seawater. In the dark, COF 2-Ru-AO showed 26.03, 24.66, 25.24, 21.31,

https://doi.org/10.1021/jacsau.2c00614
JACS Au 2023, 3, 239−251

25.52, and 48.24% inhibition of marine bacteria, *B. indicus*, *V. vulnificus*, *P. stutzeri*, *S. elongates*, and *C. sorokiniana*, respectively, suggesting reasonable intrinsic anti-biofouling activity originating from the functional groups present in the COF (Figure 5c–f and Table S11). However, under light irradiation COF 2-Ru-AO demonstrated greatly improved inhibition rates toward these marine microorganisms (96.66, 68.00, 89.53, 83.97, 89.43, and 90.35% for marine bacteria, *B. indicus*, *V. vulnificus*, *P. stutzeri*, *S. elongates*, and *C. sorokiniana*, respectively). Results demonstrate that under visible light, COF 2-Ru-AO offered impressive broad-spectrum biofouling resistance. To understand the outstanding anti-biofouling activity of COF 2-Ru-AO, radical trapping experiments and EPR were conducted to detect the possible reactive species formed during the photocatalytic process in water. Possible reactive oxygen species formed under light irradiation included $^1O_2$, $^\bullet OH$, and $^\bullet O_2^-$, which were trapped using 2,2,6,6-tetramethylpiperidine (TEMP) and 3,4-dihydro-2,3-dimethyl-2H-pyrrole 1-oxide (DMPO) (Figure 5b). No reactive oxygen species were detected under dark conditions, while $^1O_2$, $^\bullet OH$, and $^\bullet O_2^-$ all being detected under visible light irradiation. This excellent light-driven anti-biofouling activity of COF 2-Ru-AO could therefore be attributed to $^1O_2$, $^\bullet OH$, $^\bullet O_2^-$ and hole (h^+) species, which are known to damage/kill marine microorganisms.[69,71] Results show that by incorporating photoactive components in COF 2-Ru-AO and promoting effective charge separation, both efficiently U(VI) reduction to $U(IV)O_2$ and potent anti-biofouling properties were realized.

Adsorption-Photocatalytic Mechanism Study

Encouraged by the excellent uranium extraction performance of the rationally designed multicomponent COF 2-Ru-AO, we next carried out density functional theory (DFT) calculations, transient absorption spectroscopy (TAS), steady-state photoluminescence spectroscopy (PL), and time-resolved photoluminescence emission decay spectroscopy measurements to understand the chemical basis of the binding affinity and photoreducing activity of the COF toward uranyl. The calculated binding free energy of UO_2^{2+}/COF 2-Ru-AO was −29.75 kJ/mol, indicating that $[U(VI)O_2(CO_3)_3]^{4-}$ spontaneously adsorbed to the surface of the amidoxime group with the release of carbonate ions (Figure 5g). Moreover, the coordination bond lengths of U–O and U–N between amidoxime and uranyl are 2.33 and 2.54 Å, respectively (Figure S41), which are in excellent accord with the EXAFS results, further confirming the efficient and selective adsorption property of COF 2-Ru-AO for uranyl. The highest occupied molecular orbital (HOMO) and lowest unoccupied molecular orbital (LUMO) of COF 2-Ru-AO were computed to be −5.61 and −2.81 eV, respectively, in Figure 5h. This would enable efficient separation of photogenerated electrons and holes under sunlight, while also allowing photocatalytic reduction of adsorbed U(VI) to lower-valence products such as solid $U(IV)O_2$. The theoretical calculations are thus in excellent accord with our experimental findings, further confirming the efficient uranium extraction properties of COF 2-Ru-AO. Charge dynamics in COF 2-Ru-AO were studied by TAS to calculate the lifetime of the photogenerated charges (Figure 5i). Femtosecond time-resolved transient absorption decay kinetics showed a long charge carrier lifetime (τ = 1928 ps), indicating a low probability of electron–hole recombination and further explaining the high activity of COF 2-Ru-AO for uranium photoreduction. Steady-state photoluminescence spectroscopy was next used to assess charge transfer and separation in the COF photocatalysts.[54,72,73] Emission spectra of COF 1-AO and COF 2-Ru-AO were measured at an excitation wavelength of 340 nm (Figure 5j). COF 2-Ru-AO exhibited weaker photoluminescence than COF 1-AO, suggesting the $[Ru(Bp)_2Bpy]Cl_2$ component in COF 2-Ru-AO inhibited the recombination of photogenerated electrons and holes. Fitted time-resolved photoluminescence emission decay spectra showed that the calculated average lifetimes for COF 2-Ru-AO and COF 1-AO were 1.01 and 0.90 ns, respectively (Figure 5k).[74,75] These results show that the two COFs have similar average charge lifetimes, confirming that the donor (TP) and acceptor (DTz) systems are conducive to charge separation and transport, thereby enabling efficient reduction of adsorbed U(VI) to the lower-valence U(IV) product.

Results presented herein highlight the potential of reticular chemistry for building multivariate COFs as adsorption-photocatalysts for selective uranium extraction from seawater. Key design considerations utilized here included frameworks supporting amidoxime adsorption sites for selective uranyl uptake, photoactive donor–acceptor linkers and a secondary photosensitizer for efficient charge carrier generation enabling adsorbed U(VI) reduction to $U(IV)O_2$ (Figure 5l). The simultaneous generation of an assortment of reactive oxygen species under light irradiation suppressed marine biofouling. By this approach, the optimally designed COF 2-Ru-AO delivered high uranium extraction performance under visible light irradiation and good recyclability. We estimated the cost of synthesizing COF 2-Ru-AO to be ∼$3500 USD/kg, suggesting the economic feasibility of the adsorbent-photocatalyst. Moreover, the cost for uranium extraction using COF 2-Ru-AO was estimated to be ∼$1820 USD per kilogram (based on the production of 1 kg of uranium needing 0.52 kg of COF 2-Ru-AO). We anticipate that our COFs design strategy will be widely adopted in the future for selective metal sequestration from complex systems and environmental remediation.

CONCLUSIONS

In conclusion, multivariate COF adsorption-photocatalysts were developed as high-performance uranium extraction materials from seawater. COF 2-Ru-AO provided a high density of chelating amidoxime groups for selective uranyl binding with fast uranium uptake kinetics. Under visible light irradiation, the rationally designed donor–acceptor system in the COF efficiently separated electrons and holes for photoreactions (electrons causing U(VI) reduction, as well as the creation of $^1O_2$, $^\bullet OH$, and $^\bullet O_2^-$ species, while the valence holes also boosted anti-biofouling properties in seawater). Incorporation of bipyridine-Ru(II) sites in COF 2-Ru-AO further enhanced electron–hole pair generation and photocatalytic performance. These attributes made COF 2-Ru-AO an outstanding material for uranium extraction from natural seawater under visible light irradiation (importantly, without any need for sacrificial reagents). This work lays a foundation for practical uranium extraction from seawater. Results encourage the wider pursuit of adsorbent-photocatalyst COFs for uranium capture and other applications.

https://doi.org/10.1021/jacsau.2c00614
JACS Au 2023, 3, 239–251

METHODS

Instrumentation

Powder X-ray diffraction (PXRD) patterns were collected on a Rigaku SmartLab SE X-ray diffractometer equipped with a Cu Kα source. BET surface areas and pore size distributions were determined from N_2 adsorption/desorption isotherms collected at 77 K using a Micromeritics TriStar II. Samples were heated under a vacuum at 60 °C for 12 h before the measurements. Scanning electron microscopy (SEM) images were recorded on a Hitachi SU8010 (and Regulus8220) microscope. Transmission electron microscopy (TEM) images, high-angle annular dark-field scanning transmission electron microscopy (HAADF-STEM) images, energy dispersive X-ray elemental maps, and high-resolution TEM (HRTEM) images were recorded on a JEOL JEM-2100F (or JEOL JEM-F200) transmission electron microscope operating at an accelerating voltage of 200 kV. Fourier transform infrared spectra (FTIR) were recorded on a Shimadzu high-resolution IRTracer-100. ^{1}H NMR spectra were collected on a Bruker AVANCE III HD 500 spectrometer. Solid-state ^{13}C CP/MAS NMR spectra were collected on an Agilent 600M spectrometer. X-ray photoelectron spectroscopy (XPS) analyses were performed on a Thermo ESCALAB 250, fitted with a monochromated Al Kα X-ray source. Photoelectrochemical experiments were carried out using an electrochemical workstation (CHI660E) with a three-electrode electrochemical cell. Mott−Schottky plots were recorded at frequencies of 1000 Hz. Electrochemical impedance spectroscopy (EIS) data were collected in the frequency range of 0.1−100,000 Hz. The applied potential vs Ag/AgCl was converted to normal hydrogen electrode (NHE) potential using the following equation: $E_{NHE} = E_{Ag/AgCl} + E_{Ag/AgCl}^{\theta}$ ($E_{Ag/AgCl}^{\theta} = 0.199$ V). Photocurrent tests were carried out under visible light irradiation, which was generated by a 300 W xenon lamp (PerfectLight, PLS-SXE300D). Electron paramagnetic resonance (EPR) spectra were obtained on Bruker A200 and Bruker Elexsys500 spectrometers. The compound 3,4-dihydro-2,3-dimethyl-2H-pyrrole 1-oxide (DMPO) was used to trap superoxide radicals ($^{\bullet}O_2^-$) and hydroxyl radicals ($^{\bullet}$OH). The compound 2,2,6,6-tetramethylpiperidine (TEMP) was used to trap singlet oxygen ($^1O_2$). UV−vis spectra of the COFs were recorded in diffuse reflectance (DR) mode at room temperature on a SHIMADZU UV-2700 spectrophotometer equipped with an integrating sphere attachment. Thermogravimetric analyses (TGA) were carried out on a NETZSCH STA 2500 instrument. Samples were heated under an N_2 atmosphere from 25 to 800 °C at a heating rate of 10 °C/min. Inductively coupled plasma mass spectrometry (ICP-MS) analyses were performed on an Agilent 7800 spectrometer system. X-ray absorption spectra at the U L-edge were collected in transmission mode at the Shanghai Synchrotron Radiation Facility (14W station). Photoluminescence (PL) spectra were obtained at room temperature on a Hitachi F-7000 spectrofluorometer operating at an excitation wavelength of 340 nm. Time-resolved photoluminescence emission decay spectra were measured on an Edinburgh Instruments FLS 980 spectrophotometer at an excitation wavelength of 320 nm. Transient absorption spectroscopy data was obtained on a Helios pump-probe system (ultrafast systems) at $\lambda_{ex} = 490$ nm.

Synthesis of COF 1

In a 5 mL glass tube, 4,4′-(thiazolo[5,4-*d*]thiazole-2,5-diyl)dianiline (DTz, 25.9 mg), 5,5′-(diazene-1,2-diyl)bis(2-aminobenzonitrile) (DBAb, 10.5 mg), and 2,4,6-triformylphloroglucinol (TP, 16.8 mg) were dissolved in 1.1 mL of a mixed solvent solution consisting of orthodichlorobenzene (O-DCB)/1-butanol (*n*-BuOH)/acetic acid (AcOH, 6 M) with a volume ratio of 5/5/1. The mixture was frozen in a liquid nitrogen bath and sealed with a gas torch. The tube was then heated at 120 °C for 3 days, after which the product was washed several times with THF and acetone, collected by vacuum filtration, and dried under vacuum at 40 °C overnight. Elemental analysis found: C, 53.78; H, 3.38; N, 12.78; S, 10.45. The calculated linker percentage is DTz (45%), DBAb (15%), and TP (40%).

Synthesis of COF 2-Ru

In a 5 mL glass tube, [2,2′-bipyridine-5,5′-diamine-Ru(Bp)$_2$]Cl$_2$ ([Ru(Bp)$_2$Bpy]Cl$_2$, 8.04 mg), 4,4′-(thiazolo[5,4-*d*]thiazole-2,5-diyl)-dianiline (DTz, 23.4 mg), 5,5′-(diazene-1,2-diyl)bis(2-aminobenzonitrile) (DBAb, 9.4 mg), and 2,4,6-Triformylphloroglucinol (TP, 16.8 mg) were dissolved in 1.1 mL of a mixed solvent solution of O-DCB/*n*-BuOH/AcOH (6 M) with a volume ratio of 5/5/1. The mixture was frozen in a liquid nitrogen bath and sealed with a gas torch. The tube was then heated at 120 °C for 3 days, after which the product was washed several times with THF and acetone, collected by vacuum filtration, and dried under vacuum at 40 °C overnight. Elemental analysis and ICP-MS found: C, 54.4; H, 3.13; N, 10.02; S, 7.87; Ru, 0.81. The calculated linker percentage is [Ru(Bp)$_2$Bpy]Cl$_2$ (3%), DTz (34.5%), DBAb (22.5%), and TP (40%). COF 2 was synthesized via a similar synthetic route using [2,2′-bipyridine-5,5′-diamine] (Bpy, 2.23 mg) to replace the [2,2′-bipyridine-5,5′-diamine-Ru(Bp)$_2$]Cl$_2$.

Synthesis of COF 3-Ru

In a 5 mL glass tube, [2,2′-bipyridine-5,5′-diamine-Ru(Bp)$_2$]Cl$_2$ ([Ru(Bp)$_2$Bpy]Cl$_2$, 53.6 mg), 5,5′-(diazene-1,2-diyl)bis(2-aminobenzonitrile) (DBAb, 7.5 mg), and 2,4,6-triformylphloroglucinol (TP, 16.8 mg) were dissolved in 1.1 mL of a mixed solvent solution of O-DCB/n-BuOH/AcOH (6 M) with a volume ratio of 5/5/1. The mixture was frozen in a liquid nitrogen bath and sealed with a gas torch. The tube was then heated at 120 °C for 3 days, after which the product was washed several times with THF and acetone, collected by vacuum filtration, and dried under vacuum at 40 °C overnight. Elemental analysis found: C, 50.61; H, 4.08; N, 13.14. The calculated linker percentage is [Ru(Bp)$_2$Bpy]Cl$_2$ (37.5%), DBAb (22.5%), and TP (40%). COF 3 was synthesized via a similar synthetic route using [2,2′-bipyridine-5,5′-diamine] (Bpy, 14.9 mg) to replace the [2,2′-bipyridine-5,5′-diamine-Ru(Bp)$_2$]Cl$_2$.

Synthesis of COFs 1-AO, 2-AO, 2-Ru-AO, and 3-Ru-AO (AO Represents Amidoxime Groups)

For the synthesis of COF 1-AO, 0.5 g of COF 1 was dispersed in 30 mL of ethanol, followed by adding 0.4 g of $NH_2OH{\cdot}HCl$ and 0.1 mL of trimethylamine (TMA). After stirring for 18 h at 70 °C, the product was collected by filtration, washed several times with deionized water, and finally dried at 40 °C under a vacuum. COF 2-AO, COF 2-Ru-AO, and COF 3-Ru-AO were synthesized via a similar synthetic route, using COF 2, COF 2-Ru, and COF 3-Ru, respectively.

Adsorption-Photocatalytic Uranium Extraction

The performance of the COFs for the photocatalytic reduction of U(VI) solutions was evaluated in photoreactor under visible light irradiation from a 300 W xenon lamp (PerfectLight, PLS−SXE300D). COF 1-AO, 2-AO, 2-Ru-AO, or 3-Ru-AO (5 mg) was dispersed in 100 mL of spiked seawater containing ∼19 ppm U(VI). The pH of the dispersion was adjusted to ∼8.1 using Na_2CO_3, thus closely approximating seawater in pH and carbonate concentration. The dispersion was stirred in dark for 24 h before irradiation. Next, the reactor was continuously exposed to the Xe lamp. At regular intervals, aliquots of the dispersion were removed and filtered through a 0.45 μm membrane filter. The concentration of U(VI) in the filtrates was measured by UV−vis spectrophotometry at a wavelength of 650 nm using the Arsenazo III method. After uranium adsorption-photocatalysis experiments, COF 2-Ru-AO was sonicated, centrifugation, filtered, and washed with HNO_3 (pH = 3)/$NaNO_3$ solutions and distilled water. Then, the solid catalyst was subsequently returned to the photoreactor for further adsorption-photocatalytic tests. Further photocatalytic experiments were conducted using natural seawater. The seawater used in the work was collected in the South China Sea and then filtered to remove insoluble substances such as particulates. COF 2-Ru-AO (10 mg) was spread on the top of a column filled with sea sand, then the seawater (∼40 L) cycled in a continuous loop through the column from top to bottom. The Xe lamp irradiated the COF 2-Ru-AO with visible light irradiation from above. The filtrate at

https://doi.org/10.1021/jacsau.2c00614
JACS Au 2023, 3, 239−251

the bottom of the sand column was analyzed periodically using ICP-MS to quantify the remaining metal-ion content.

■ ASSOCIATED CONTENT

Supporting Information

The Supporting Information is available free of charge at https://pubs.acs.org/doi/10.1021/jacsau.2c00614.

Chemicals, additional experimental procedures, anti-biofouling measurements, and additional materials characterization (FTIR, PXRD, TGA, SEM, EDS, TEM, gas sorption analysis, pore size distribution calculations, UV−visible diffuse reflectance spectroscopy, solid-state ^{13}C CP/MAS NMR, XPS, XAS, DFT calculation, and adsorption calculations) (PDF)

■ AUTHOR INFORMATION

Corresponding Authors

Hui Yang − *College of Environmental Science and Engineering, North China Electric Power University, Beijing 102206, P. R. China;* orcid.org/0000-0002-6745-642X; Email: h.yang@ncepu.edu.cn

Shengqian Ma − *Department of Chemistry, University of North Texas, Denton, Texas 76201, United States;* orcid.org/0000-0002-1897-7069; Email: xkwang@ncepu.edu.cn

Xiangke Wang − *College of Environmental Science and Engineering, North China Electric Power University, Beijing 102206, P. R. China;* orcid.org/0000-0002-3352-1617; Email: shengqian.ma@unt.edu

Authors

Mengjie Hao − *College of Environmental Science and Engineering, North China Electric Power University, Beijing 102206, P. R. China*

Yinghui Xie − *College of Environmental Science and Engineering, North China Electric Power University, Beijing 102206, P. R. China*

Xiaolu Liu − *College of Environmental Science and Engineering, North China Electric Power University, Beijing 102206, P. R. China*

Zhongshan Chen − *College of Environmental Science and Engineering, North China Electric Power University, Beijing 102206, P. R. China*

Geoffrey I. N. Waterhouse − *MacDiarmid Institute for Advanced Materials and Nanotechnology, School of Chemical Sciences, The University of Auckland, Auckland 1142, New Zealand;* orcid.org/0000-0002-3296-3093

Complete contact information is available at: https://pubs.acs.org/10.1021/jacsau.2c00614

Author Contributions

All authors have given approval to the final version of the manuscript. CRediT: **Mengjie Hao** conceptualization, formal analysis, investigation, software, writing-original draft; **Yinghui Xie** data curation, formal analysis, investigation, software; **Xiaolu Liu** data curation, formal analysis, investigation, software; **Zhongshan Chen** data curation, formal analysis, methodology; **Hui Yang** funding acquisition, project administration, supervision, writing-original draft, writing-review & editing; **Geoffrey I.N. Waterhouse** writing-review & editing; **Shengqian Ma** validation, writing-review & editing; **Xiangke Wang** funding acquisition, supervision, writing-review & editing.

Notes

The authors declare no competing financial interest.

■ ACKNOWLEDGMENTS

The authors gratefully acknowledge funding support from the National Science Foundation of China (Grants U2167218; 22006036), National Key Research and Development Program of China (2018YFC1900105), the Beijing Outstanding Young Scientist Program (H.Y. and X.W.), and the Robert A. Welch Foundation (B-0027) (S.M.). G.I.N.W. was supported by a James Cook Research Fellowship from New Zealand Government funding, administered by the Royal Society Te Apārangi. The authors also acknowledge support from the 14W station in Shanghai Synchrotron Radiation Facility (SSRF).

■ REFERENCES

(1) Adamantiades, A.; Kessides, I. Nuclear Power for Sustainable Development: Current Status and Future Prospects. *Energy Policy* **2009**, *37*, 5149−5166.

(2) Mayer, K.; Wallenius, M.; Lutzenkirchen, K.; Horta, J.; Nicholl, A.; Rasmussen, G.; van Belle, P.; Varga, Z.; Buda, R.; Erdmann, N.; Kratz, J. V.; Trautmann, N.; Fifield, L. K.; Tims, S. G.; Frohlich, M. B.; Steier, P. Uranium from German Nuclear Power Projects of the 1940s-A Nuclear Forensic Investigation. *Angew. Chem., Int. Ed.* **2015**, *54*, 13452−13456.

(3) Sholl, D. S.; Lively, R. P. Seven Chemical Separations to Change the World. *Nature* **2016**, *532*, 435−437.

(4) Kim, J.; Tsouris, C.; Mayes, R. T.; Oyola, Y.; Saito, T.; Janke, C. J.; Dai, S.; Schneider, E.; Sachde, D. Recovery of Uranium from Seawater: A Review of Current Status and Future Research Needs. *Sep. Sci. Technol.* **2013**, *48*, 367−387.

(5) Lindner, H.; Schneider, E. Review of Cost Estimates for Uranium Recovery from Seawater. *Energy Econ.* **2015**, *49*, 9−22.

(6) Shao, D.; Hou, G.; Li, J.; Wen, T.; Ren, X.; Wang, X. PANI/GO as a Super Adsorbent for the Selective Adsorption of Uranium(VI). *Chem. Eng. J.* **2014**, *255*, 604−612.

(7) Liu, C.; Hsu, P.-C.; Xie, J.; Zhao, J.; Wu, T.; Wang, H.; Liu, W.; Zhang, J.; Chu, S.; Cui, Y. A Half-Wave Rectified Alternating Current Electrochemical Method for Uranium Extraction from Seawater. *Nat. Energy* **2017**, *2*, No. 17007.

(8) Ismail, A. F.; Yim, M.-S. Investigation of Activated Carbon Adsorbent Electrode for Electrosorption-Based Uranium Extraction from Seawater. *Nucl. Eng. Technol.* **2015**, *47*, 579−587.

(9) Yang, H.; Liu, X.; Hao, M.; Xie, Y.; Wang, X.; Tian, H.; Waterhouse, G. I. N.; Kruger, P. E.; Telfer, S. G.; Ma, S. Functionalized Iron-Nitrogen-Carbon Electrocatalyst Provides a Reversible Electron Transfer Platform for Efficient Uranium Extraction from Seawater. *Adv. Mater.* **2021**, *33*, No. 2106621.

(10) Wang, F.; Li, H.; Liu, Q.; Li, Z.; Li, R.; Zhang, H.; Liu, L.; Emelchenko, G. A.; Wang, J. A Graphene Oxide/Amidoxime Hydrogel for Enhanced Uranium Capture. *Sci. Rep.* **2016**, *6*, No. 19367.

(11) Li, N.; Yang, L.; Wang, D.; Tang, C.; Deng, W.; Wang, Z. High-Capacity Amidoxime-Functionalized beta-Cyclodextrin/Graphene Aerogel for Selective Uranium Capture. *Environ. Sci. Technol.* **2021**, *55*, 9181−9188.

(12) Yue, Y.; Sun, X.; Mayes, R. T.; Kim, J.; Fulvio, P. F.; Qiao, Z.; Brown, S.; Tsouris, C.; Oyola, Y.; Dai, S. Polymer-Coated Nanoporous Carbons for Trace Seawater Uranium Adsorption. *Sci. China Chem.* **2013**, *56*, 1510−1515.

(13) Feng, M. L.; Sarma, D.; Qi, X. H.; Du, K. Z.; Huang, X. Y.; Kanatzidis, M. G. Efficient Removal and Recovery of Uranium by a Layered Organic-Inorganic Hybrid Thiostannate. *J. Am. Chem. Soc.* **2016**, *138*, 12578−12585.

(14) Yue, Y.; Mayes, R. T.; Kim, J.; Fulvio, P. F.; Sun, X. G.; Tsouris, C.; Chen, J.; Brown, S.; Dai, S. Seawater Uranium Sorbents: Preparation from a Mesoporous Copolymer Initiator by Atom-Transfer Radical Polymerization. *Angew. Chem., Int. Ed.* **2013**, *52*, 13458−13462.
(15) Das, S.; Brown, S.; Mayes, R. T.; Janke, C. J.; Tsouris, C.; Kuo, L. J.; Gill, G.; Dai, S. Novel Poly(imide dioxime) Sorbents: Development and Testing for Enhanced Extraction of Uranium from Natural Seawater. *Chem. Eng. J.* **2016**, *298*, 125−135.
(16) Pan, H.-B.; Kuo, L.-J.; Wood, J.; Strivens, J.; Gill, G. A.; Janke, C. J.; Wai, C. M. Towards Understanding KOH Conditioning of Amidoxime-Based Polymer Adsorbents for Sequestering Uranium from Seawater. *RSC Adv.* **2015**, *5*, 100715−100721.
(17) Yuan, Y.; Yang, Y.; Ma, X.; Meng, Q.; Wang, L.; Zhao, S.; Zhu, G. Molecularly Imprinted Porous Aromatic Frameworks and Their Composite Components for Selective Extraction of Uranium Ions. *Adv. Mater.* **2018**, *30*, No. 1706507.
(18) Alexandratos, S. D.; Zhu, X.; Florent, M.; Sellin, R. Polymer-Supported Bifunctional Amidoximes for the Sorption of Uranium from Seawater. *Ind. Eng. Chem. Res.* **2016**, *55*, 4208−4216.
(19) Kuo, L.-J.; Janke, C. J.; Wood, J. R.; Strivens, J. E.; Das, S.; Oyola, Y.; Mayes, R. T.; Gill, G. A. Characterization and Testing of Amidoxime-Based Adsorbent Materials to Extract Uranium from Natural Seawater. *Ind. Eng. Chem. Res.* **2016**, *55*, 4285−4293.
(20) Brown, S.; Yue, Y.; Kuo, L.-J.; Mehio, N.; Li, M.; Gill, G.; Tsouris, C.; Mayes, R. T.; Saito, T.; Dai, S. Uranium Adsorbent Fibers Prepared by Atom-Transfer Radical Polymerization (ATRP) from Poly(vinyl chloride)-co-chlorinated Poly(vinyl chloride) (PVC-co-CPVC) Fiber. *Ind. Eng. Chem. Res.* **2016**, *55*, 4139−4148.
(21) Yang, L.; Xiao, H.; Qian, Y.; Zhao, X.; Kong, X.-Y.; Liu, P.; Xin, W.; Fu, L.; Jiang, L.; Wen, L. Bioinspired Hierarchical Porous Membrane for Efficient Uranium Extraction from Seawater. *Nat. Sustain.* **2022**, *5*, 71−80.
(22) Xu, X.; Zhang, H.; Ao, J.; Xu, L.; Liu, X.; Guo, X.; Li, J.; Zhang, L.; Li, Q.; Zhao, X.; Ye, B.; Wang, D.; Shen, F.; Ma, H. 3D Hierarchical Porous Amidoxime Fibers Speed up Uranium Extraction from Seawater. *Energy Environ. Sci.* **2019**, *12*, 1979−1988.
(23) Sun, Q.; Aguila, B.; Perman, J.; Ivanov, A. S.; Bryantsev, V. S.; Earl, L. D.; Abney, C. W.; Wojtas, L.; Ma, S. Bio-Inspired Nano-Traps for Uranium Extraction from Seawater and Recovery from Nuclear Waste. *Nat. Commun.* **2018**, *9*, No. 1644.
(24) Sun, Q.; Song, Y.; Aguila, B.; Ivanov, A. S.; Bryantsev, V. S.; Ma, S. Spatial Engineering Direct Cooperativity between Binding Sites for Uranium Sequestration. *Adv. Sci.* **2021**, *8*, No. 2001573.
(25) Yuan, Y.; Meng, Q.; Faheem, M.; Yang, Y.; Li, Z.; Wang, Z.; Deng, D.; Sun, F.; He, H.; Huang, Y.; Sha, H.; Zhu, G. A Molecular Coordination Template Strategy for Designing Selective Porous Aromatic Framework Materials for Uranyl Capture. *ACS Cent. Sci.* **2019**, *5*, 1432−1439.
(26) Odoh, S. O.; Bondarevsky, G. D.; Karpus, J.; Cui, Q.; He, C.; Spezia, R.; Gagliardi, L. UO_2^{2+} Uptake by Proteins: Understanding the Binding Features of the Super Uranyl Binding Protein and Design of a Protein with Higher Affinity. *J. Am. Chem. Soc.* **2014**, *136*, 17484−17494.
(27) Zhou, L.; Bosscher, M.; Zhang, C.; Ozcubukcu, S.; Zhang, L.; Zhang, W.; Li, C. J.; Liu, J.; Jensen, M. P.; Lai, L.; He, C. A Protein Engineered to Bind Uranyl Selectively and with Femtomolar Affinity. *Nat. Chem.* **2014**, *6*, 236−241.
(28) Yuan, Y.; Liu, T.; Xiao, J.; Yu, Q.; Feng, L.; Niu, B.; Feng, S.; Zhang, J.; Wang, N. DNA Nano-Pocket for Ultra-Selective Uranyl Extraction from Seawater. *Nat. Commun.* **2020**, *11*, No. 5708.
(29) Liu, W.; Dai, X.; Bai, Z.; Wang, Y.; Yang, Z.; Zhang, L.; Xu, L.; Chen, L.; Li, Y.; Gui, D.; Diwu, J.; Wang, J.; Zhou, R.; Chai, Z.; Wang, S. Highly Sensitive and Selective Uranium Detection in Natural Water Systems Using a Luminescent Mesoporous Metal-Organic Framework Equipped with Abundant Lewis Basic Sites: A Combined Batch, X-ray Absorption Spectroscopy, and First Principles Simulation Investigation. *Environ. Sci. Technol.* **2017**, *51*, 3911−3921.
(30) Chen, L.; Bai, Z.; Zhu, L.; Zhang, L.; Cai, Y.; Li, Y.; Liu, W.; Wang, Y.; Chen, L.; Diwu, J.; Wang, J.; Chai, Z.; Wang, S. Ultrafast and Efficient Extraction of Uranium from Seawater Using an Amidoxime Appended Metal-Organic Framework. *ACS. Appl. Mater. Interfaces* **2017**, *9*, 32446−32451.
(31) Li, H.; Zhai, F.; Gui, D.; Wang, X.; Wu, C.; Zhang, D.; Dai, X.; Deng, H.; Su, X.; Diwu, J.; Lin, Z.; Chai, Z.; Wang, S. Powerful Uranium Extraction Strategy with Combined Ligand Complexation and Photocatalytic Reduction by Postsynthetically Modified Photoactive Metal-Organic Frameworks. *Appl. Catal., B* **2019**, *254*, 47−54.
(32) Bai, Z.-Q.; Yuan, L.-Y.; Zhu, L.; Liu, Z.-R.; Chu, S.-Q.; Zheng, L.-R.; Zhang, J.; Chai, Z.-F.; Shi, W.-Q. Introduction of Amino Groups into Acid-Resistant MOFs for Enhanced $U_{(VI)}$ Sorption. *J. Mater. Chem. A* **2015**, *3*, 525−534.
(33) Zhang, J.; Zhang, H.; Liu, Q.; Song, D.; Li, R.; Liu, P.; Wang, J. Diaminomaleonitrile Functionalized Double-Shelled Hollow MIL-101 (Cr) for Selective Removal of Uranium from Simulated Seawater. *Chem. Eng. J.* **2019**, *368*, 951−958.
(34) Mollick, S.; Saurabh, S.; More, Y. D.; Fajal, S.; Shirolkar, M. M.; Mandal, W.; Ghosh, S. K. Benchmark Uranium Extraction from Seawater Using an Ionic Macroporous Metal−Organic Framework. *Energy Environ. Sci.* **2022**, *15*, 3462−3469.
(35) Li, Y.; Chen, W.; Xing, G.; Jiang, D.; Chen, L. New Synthetic Strategies Toward Covalent Organic Frameworks. *Chem. Soc. Rev.* **2020**, *49*, 2852−2868.
(36) Wang, H.; Wang, H.; Wang, Z.; Tang, L.; Zeng, G.; Xu, P.; Chen, M.; Xiong, T.; Zhou, C.; Li, X.; Huang, D.; Zhu, Y.; Wang, Z.; Tang, J. Covalent Organic Framework Photocatalysts: Structures and Applications. *Chem. Soc. Rev.* **2020**, *49*, 4135−4165.
(37) Wang, Z.; Zhang, S.; Chen, Y.; Zhang, Z.; Ma, S. Covalent Organic Frameworks For Separation Applications. *Chem. Soc. Rev.* **2020**, *49*, 708−735.
(38) Liu, X.; Pang, H.; Liu, X.; Li, Q.; Zhang, N.; Mao, L.; Qiu, M.; Hu, B.; Yang, H.; Wang, X. Orderly Porous Covalent Organic Frameworks-Based Materials: Superior Adsorbents for Pollutants Removal from Aqueous Solutions. *The Innovation* **2021**, *2*, No. 100076.
(39) Li, Y.; Guo, X.; Li, X.; Zhang, M.; Jia, Z.; Deng, Y.; Tian, Y.; Li, S.; Ma, L. Redox-Active Two-Dimensional Covalent Organic Frameworks (COFs) for Selective Reductive Separation of Valence-Variable, Redox-Sensitive and Long-Lived Radionuclides. *Angew. Chem., Int. Ed.* **2020**, *59*, 4168−4175.
(40) Gropp, C.; Ma, T.; Hanikel, N.; Yaghi, O. M. Design of Higher Valency in Covalent Organic Frameworks. *Science* **2020**, *370*, 6406.
(41) Lyle, S. J.; Waller, P. J.; Yaghi, O. M. Covalent Organic Frameworks: Organic Chemistry Extended into Two and Three Dimensions. *Trends Chem.* **2019**, *1*, 172−184.
(42) Tang, N.; Liang, J.; Niu, C.; Wang, H.; Luo, Y.; Xing, W.; Ye, S.; Liang, C.; Guo, H.; Guo, J.; Zhang, Y.; Zeng, G. Amidoxime-based materials for uranium recovery and removal. *J. Mater. Chem. A* **2020**, *8*, 7588−7625.
(43) Cui, W. R.; Li, F. F.; Xu, R. H.; Zhang, C. R.; Chen, X. R.; Yan, R. H.; Liang, R. P.; Qiu, J. D. Regenerable Covalent Organic Frameworks for Photo-Enhanced Uranium Adsorption from Seawater. *Angew. Chem., Int. Ed.* **2020**, *59*, 17684−17690.
(44) Sun, Q.; Aguila, B.; Earl, L. D.; Abney, C. W.; Wojtas, L.; Thallapally, P. K.; Ma, S. Covalent Organic Frameworks as a Decorating Platform for Utilization and Affinity Enhancement of Chelating Sites for Radionuclide Sequestration. *Adv. Mater.* **2018**, *30*, No. 1705479.
(45) Biswal, B. P.; Vignolo-Gonzalez, H. A.; Banerjee, T.; Grunenberg, L.; Savasci, G.; Gottschling, K.; Nuss, J.; Ochsenfeld, C.; Lotsch, B. V. Sustained Solar H_2 Evolution from a Thiazolo[5,4-d]thiazole-Bridged Covalent Organic Framework and Nickel-Thiolate Cluster in Water. *J. Am. Chem. Soc.* **2019**, *141*, 11082−11092.
(46) Ghosh, S.; Nakada, A.; Springer, M. A.; Kawaguchi, T.; Suzuki, K.; Kaji, H.; Baburin, I.; Kuc, A.; Heine, T.; Suzuki, H.; Abe, R.; Seki, S. Identification of Prime Factors to Maximize the Photocatalytic

https://doi.org/10.1021/jacsau.2c00614
JACS Au 2023, 3, 239−251

Hydrogen Evolution of Covalent Organic Frameworks. *J. Am. Chem. Soc.* **2020**, *142*, 9752−9762.
(47) Gottschling, K.; Savasci, G.; Vignolo-Gonzalez, H.; Schmidt, S.; Mauker, P.; Banerjee, T.; Rovo, P.; Ochsenfeld, C.; Lotsch, B. V. Rational Design of Covalent Cobaloxime-Covalent Organic Framework Hybrids for Enhanced Photocatalytic Hydrogen Evolution. *J. Am. Chem. Soc.* **2020**, *142*, 12146−12156.
(48) Liu, W.; Li, X.; Wang, C.; Pan, H.; Liu, W.; Wang, K.; Zeng, Q.; Wang, R.; Jiang, J. A Scalable General Synthetic Approach toward Ultrathin Imine-Linked Two-Dimensional Covalent Organic Framework Nanosheets for Photocatalytic CO_2 Reduction. *J. Am. Chem. Soc.* **2019**, *141*, 17431−17440.
(49) Qian, Y.; Li, D.; Han, Y.; Jiang, H. L. Photocatalytic Molecular Oxygen Activation by Regulating Excitonic Effects in Covalent Organic Frameworks. *J. Am. Chem. Soc.* **2020**, *142*, 20763−20771.
(50) Wan, Y.; Wang, L.; Xu, H.; Wu, X.; Yang, J. A Simple Molecular Design Strategy for Two-Dimensional Covalent Organic Framework Capable of Visible-Light-Driven Water Splitting. *J. Am. Chem. Soc.* **2020**, *142*, 4508−4516.
(51) Wei, S.; Zhang, F.; Zhang, W.; Qiang, P.; Yu, K.; Fu, X.; Wu, D.; Bi, S.; Zhang, F. Semiconducting 2D Triazine-Cored Covalent Organic Frameworks with Unsubstituted Olefin Linkages. *J. Am. Chem. Soc.* **2019**, *141*, 14272−14279.
(52) Huang, W.; He, Q.; Hu, Y.; Li, Y. Molecular Heterostructures of Covalent Triazine Frameworks for Enhanced Photocatalytic Hydrogen Production. *Angew. Chem., Int. Ed.* **2019**, *58*, 8676−8680.
(53) Hao, M.; Chen, Z.; Liu, X.; Liu, X.; Zhang, J.; Yang, H.; Waterhouse, G. I. N.; Wang, X.; Ma, S. Converging Cooperative Functions into the Nanospace of Covalent Organic Frameworks for Efficient Uranium Extraction from Seawater. *CCS Chem.* **2022**, *4*, 2294−2307.
(54) Li, W.; Huang, X.; Zeng, T.; Liu, Y. A.; Hu, W.; Yang, H.; Zhang, Y. B.; Wen, K. Thiazolo[5,4-d]thiazole-Based Donor-Acceptor Covalent Organic Framework for Sunlight-Driven Hydrogen Evolution. *Angew. Chem., Int. Ed.* **2021**, *60*, 1869−1874.
(55) Zhou, T.; Wang, L.; Huang, X.; Unruangsri, J.; Zhang, H.; Wang, R.; Song, Q.; Yang, Q.; Li, W.; Wang, C.; Takahashi, K.; Xu, H.; Guo, J. PEG-Stabilized Coaxial Stacking of Two-Dimensional Covalent Organic Frameworks for Enhanced Photocatalytic Hydrogen Evolution. *Nat. Commun.* **2021**, *12*, No. 3934.
(56) Li, R. L.; Yang, A.; Flanders, N. C.; Yeung, M. T.; Sheppard, D. T.; Dichtel, W. R. Two-Dimensional Covalent Organic Framework Solid Solutions. *J. Am. Chem. Soc.* **2021**, *143*, 7081−7087.
(57) Pang, Z. F.; Xu, S. Q.; Zhou, T. Y.; Liang, R. R.; Zhan, T. G.; Zhao, X. Construction of Covalent Organic Frameworks Bearing Three Different Kinds of Pores through the Heterostructural Mixed Linker Strategy. *J. Am. Chem. Soc.* **2016**, *138*, 4710−4713.
(58) Huang, N.; Zhai, L.; Coupry, D. E.; Addicoat, M. A.; Okushita, K.; Nishimura, K.; Heine, T.; Jiang, D. Multiple-Component Covalent Organic Frameworks. *Nat. Commun.* **2016**, *7*, No. 12325.
(59) Kandambeth, S.; Mallick, A.; Lukose, B.; Mane, M. V.; Heine, T.; Banerjee, R. Construction of Crystalline 2D Covalent Organic Frameworks with Remarkable Chemical (Acid/Base) Stability via a Combined Reversible and Irreversible Route. *J. Am. Chem. Soc.* **2012**, *134*, 19524−19527.
(60) Biswal, B. P.; Chandra, S.; Kandambeth, S.; Lukose, B.; Heine, T.; Banerjee, R. Mechanochemical Synthesis of Chemically Stable Isoreticular Covalent Organic Frameworks. *J. Am. Chem. Soc.* **2013**, *135*, 5328−5331.
(61) Akkermans, R. L. C.; Spenley, N. A.; Robertson, S. H. Monte Carlo Methods in Materials Studio. *Mol. Simul.* **2013**, *39*, 1153−1164.
(62) Kumar, G.; Singh, M.; Goswami, R.; Neogi, S. Structural Dynamism-Actuated Reversible CO_2 Adsorption Switch and Post-metalation-Induced Visible Light Calpha-H Photocyanation with Rare Size Selectivity in N-Functionalized 3D Covalent Organic Framework. *ACS. Appl. Mater. Interfaces* **2020**, *12*, 48642−48653.
(63) Song, Y.; Li, Z.; Zhu, Y.; Feng, X.; Chen, J. S.; Kaufmann, M.; Wang, C.; Lin, W. Titanium Hydroxide Secondary Building Units in Metal-Organic Frameworks Catalyze Hydrogen Evolution under Visible Light. *J. Am. Chem. Soc.* **2019**, *141*, 12219−12223.
(64) Lu, C.; Zhang, P.; Jiang, S.; Wu, X.; Song, S.; Zhu, M.; Lou, Z.; Li, Z.; Liu, F.; Liu, Y.; Wang, Y.; Le, Z. Photocatalytic Reduction Elimination of UO_2^{2+} Pollutant Under Visible Light with Metal-Free Sulfur Doped g-C_3N_4 Photocatalyst. *Appl. Catal., B* **2017**, *200*, 378−385.
(65) Vukovic, S.; Watson, L. A.; Kang, S. O.; Custelcean, R.; Hay, B. P. How Amidoximate Binds the Uranyl Cation. *Inorg. Chem.* **2012**, *51*, 3855−3859.
(66) Yuan, Y.; Niu, B.; Yu, Q.; Guo, X.; Guo, Z.; Wen, J.; Liu, T.; Zhang, H.; Wang, N. Photoinduced Multiple Effects to Enhance Uranium Extraction from Natural Seawater by Black Phosphorus Nanosheets. *Angew. Chem., Int. Ed.* **2020**, *59*, 1220−1227.
(67) Yuan, Y.; Yu, Q.; Cao, M.; Feng, L.; Feng, S.; Liu, T.; Feng, T.; Yan, B.; Guo, Z.; Wang, N. Selective Extraction of Uranium from Seawater with Biofouling-Resistant Polymeric Peptide. *Nat. Sustain.* **2021**, *4*, 708−714.
(68) Wang, D.; Song, J.; Lin, S.; Wen, J.; Ma, C.; Yuan, Y.; Lei, M.; Wang, X.; Wang, N.; Wu, H. A Marine-Inspired Hybrid Sponge for Highly Efficient Uranium Extraction from Seawater. *Adv. Funct. Mater.* **2019**, *29*, No. 1901009.
(69) He, N.; Cao, S.; Zhang, L.; Tian, Z.; Chen, H.; Jiang, F. Enhanced Photocatalytic Disinfection of *Escherichia coli* K-12 by Porous g-C_3N_4 Nanosheets: Combined Effect of Photo-Generated and Intracellular ROSs. *Chemosphere* **2019**, *235*, 1116−1124.
(70) Fukushima, M.; Tatsumi, K.; Tanaka, S.; Nakamura, H. Photocatalytic Production of Hydrogen Peroxide by Tris(2,2'-bipyridine) Ruthenium(II) Using Humic Acids as Electron Donor. *Environ. Sci. Technol.* **1998**, *32*, 3948−3953.
(71) Li, H.; Zhong, J.; Zhu, H.; Yang, Y.; Ding, M.; Luo, L.; Huo, Y.; Li, H. Hybrid Cu_2O/TiO_2 Nanocomposites with Enhanced Photocatalytic Antibacterial Activity toward Acinetobacter Baumannii. *ACS Appl. Bio. Mater.* **2019**, *2*, 4892−4903.
(72) Wang, H.; Qian, C.; Liu, J.; Zeng, Y.; Wang, D.; Zhou, W.; Gu, L.; Wu, H.; Liu, G.; Zhao, Y. Integrating Suitable Linkage of Covalent Organic Frameworks into Covalently Bridged Inorganic/Organic Hybrids toward Efficient Photocatalysis. *J. Am. Chem. Soc.* **2020**, *142*, 4862−4871.
(73) Guo, S.; Kong, L. H.; Wang, P.; Yao, S.; Lu, T. B.; Zhang, Z. M. Switching Excited State Distribution of Metal-Organic Framework for Dramatically Boosting Photocatalysis. *Angew. Chem., Int. Ed.* **2022**, *61*, No. 202206193.
(74) Ding, X.; Chen, L.; Honsho, Y.; Feng, X.; Saengsawang, O.; Guo, J.; Saeki, A.; Seki, S.; Irle, S.; Nagase, S.; Parasuk, V.; Jiang, D. An n-channel Two-Dimensional Covalent Organic Framework. *J. Am. Chem. Soc.* **2011**, *133*, 14510−14513.
(75) Xu, J.; Yang, C.; Bi, S.; Wang, W.; He, Y.; Wu, D.; Liang, Q.; Wang, X.; Zhang, F. Vinylene-Linked Covalent Organic Frameworks (COFs) with Symmetry-Tuned Polarity and Photocatalytic Activity. *Angew. Chem., Int. Ed.* **2020**, *59*, 23845−23853.

https://doi.org/10.1021/jacsau.2c00614
JACS Au 2023, 3, 239−251